Fouling Thresholds in Bare Tubes and Tubes Fitted with Inserts

Mengyan Yang* and Barry Crittenden

Department of Chemical Engineering, University of Bath, Bath, BA2 7AY, United Kingdom

Corresponding author. Email: my223@bath.ac.uk
Tel: +44(0) 1225 386501
Fax. +44(0) 1225 385713

Abstract

Maya crude oil fouling reveals a straightforward dependency of initial fouling rate on surface temperature but a rather complex dependency on velocity in bare tubes, the initial fouling rate showing a maximum and then decreasing significantly towards zero as the velocity is increased. Surface shear stress clearly is an important parameter. CFD simulation of fluid flow in a tube fitted with a hiTRAN® insert reveals a complex distribution of surface shear stress. To compare the insert situation with the bare tube, an equivalent velocity concept is introduced on the basis that at a given average velocity the fluid flow results in the same average wall shear stress regardless of whether the tube is bare or is fitted with an insert. Using the equivalent velocity concept, the fouling data obtained using both a bare tube and a tube fitted with inserts can be correlated using a single model. Moreover, the fouling threshold conditions below which fouling is negligible, can be predicted for both situations.

Key Words fouling; threshold conditions; crude oil; hiTRAN® inserts; CFD

1 Introduction

Most recent research on threshold conditions have been of the fouling on the inside surface of a bare round tube. Indeed, very limited work has addressed fouling threshold conditions in more complex geometries. Fouling threshold models [1, 2] can be difficult to use for predicting fouling rates for different operating conditions and crude oil types, and even more difficult for different configurations of heat exchanger surface. Based on the model developed by Epstein [3],Yeap et al. [4] proposed a model for bare round tubes incorporating the effects of mass transport and chemical reaction. A fouling suppression term, $Cu^{0.8}$, was included such that the model would be capable of predicting not only fouling threshold conditions as a function of velocity but also maxima in the fouling rate – velocity relationship [5, 6]. hiTRAN® in-tube inserts have been shown to be effective in mitigating crude oil fouling [7, 8] and increasing interest in their use in such applications is being shown by the oil industry [9] as well as by the water industries [10, 11]. A good review of applications and benefits of tube inserts in heat exchangers is provided by Ritchie and Droegemueller [8]. Ritchie et al. [12] studied the characteristics of fluid flow in the tube with inserts, and indicated that the flow near the wall resembled a turbulent profile even at a Reynolds number of 500. They also gave some theoretical analysis of the fouling on the wall of tube with inserts, auguring well for the development of suitable models for fouling of tubes containing inserts [12].

The use of inserts, however, raises a challenge in the application of fouling models, namely in the determination of Reynolds number and wall shear stress. Indeed, current fouling models are not capable of taking into account the complex variation of surface shear stress along the insert length. Whilst wall shear stress is easily calculated for bare round tubes using the friction factor approach, this method cannot be used with hiTRAN® inserts. The objective of this work therefore is to determine whether CFD simulation can offer a possible solution to this challenge such that a suitably modified fouling model can be used to predict the fouling rate and threshold conditions for tubes with and without inserts fitted.

2 Experiments and CFD simulation

2.1 Fouling Experiments

Details of the experimental rig, the crude oil, the procedure and results with bare tubes are provided by Crittenden et al. [6]. The rig, as shown in Figure 1, comprised a 0.105 m^3 heated reservoir, a variable speed centrifugal feed pump and a by-pass for circulating crude oil through the reservoir whilst the oil was being heated. Flow rates to two 270mm parallel tubular test sections were individually controlled and monitored using rotameters. Three surface thermocouples were used to record tube surface temperatures. The apparatus was

maintained at a constant pressure of 15 bar and the crude oil temperature was maintained constant at 150°C. Surface temperatures up to 280°C were obtained by constant flux direct electrical heating. Unfiltered Maya crude oil was selected for study since it was expected to foul easily and because it contained a low percentage of light ends, making it easier to handle in the laboratory [6]. Typical properties were 21.1 API gravity, vapour pressure in the range 6.2-6.7 psig, 0.55% gas w/w, 4.03% total wax w/w, -21°C pour point, a calculated cloud point in the range 17-40°C, and viscosities of 161.5 and 54.80 mm^2/s at 30°C and 50°C, respectively. The overall composition of Maya crude oil and its physical properties are provided elsewhere [6, 13]. Its fluid properties were assumed to remain constant from run to run. The hiTRAN® tube inserts were provided by Cal Gavin Ltd (Alcester, UK; www.calgavin.com). Most experiments were conducted using a "medium density" insert signified as MDI in Table 1. The medium density inserts consist of about 420 wire loops per metre. The loop is of 12.2 mm diameter and made of 0.76 mm diameter stainless steel wire. The loop matrix occupied the entire test section.

Details of the fouling resistance, fouling rate, and their calculations can be found elsewhere [5, 13], but a brief description is as follows. By definition a heat flux (W/m^2) is driven by a temperature difference (K) to overcome an overall thermal resistance, R:

$$heat\ flux = \frac{\Delta T}{R}$$

where the thermal resistance takes the unit Km^2W^{-1}. The overall thermal resistance is a sum of the original thermal resistance of the system and an additional resistance due to fouling, i.e. the fouling resistance, R_f , which therefore has the same unit as of R. The fouling rate is defined as the change of thermal resistance per unit time. Here hours are used because fouling is slow, and therefore the unit for fouling rate is $Km^2W^{-1}h^{-1}$.

2.2 CFD Simulation

The CFD package Comsol (Burlington, MA, USA) is used to model the distributions of wall shear stress in bare tubes and tubes with the insert. The equations of the k-ε turbulence flow model can be found elsewhere [14, 15]. For the bare tube, the geometry is taken to be two-dimensional with axial symmetry, whilst for the tube fitted with the insert, the geometry must be considered to be three-dimensional. As shown in the Cal Gavin web site (www.calgavin.com), hiTRAN® inserts comprise a series of loops equally spaced with a helical pattern and periodical pattern in the axial dimension. For CFD, the inserts are represented by closed round loops whose diameter and thickness are set to be the same as for the actual insert. In the CFD, the loops are placed in a cylinder so that the actual situation is closely simulated. The boundary conditions are set to be a logarithmic wall function for all walls, a constant linear velocity for the inlet and an open boundary for the outlet. The simulations were conducted for average inlet velocities in the range of the experimental values shown in Table 1. Under the conditions listed in Table 1, the fluid flow in the tube with inserts is in turbulent mode according to the study by Ritchie et al. [8]. The mesh size at the boundaries was set to be much smaller than in the bulk fluid. A series of simulations was conducted, beginning with a coarse mesh and then refined until the resulting velocity field and the velocity gradient near the wall were virtually independent of the mesh size. Further mesh refining caused significantly longer computational times.

3 Results and discussions

3.1 Experimental results – bare tube and tube with insert

As reported elsewhere [6], the average linear initial fouling rate was calculated using changes with time in the surface temperatures recorded by the thermocouples. Fouling rates at various

initial surface temperatures with the bare tube are shown as a function of velocity in Figure 2. A maximum in the fouling rate as a function of velocity was also observed with experiments using a model chemical system of styrene polymerization [5]. As the velocity approaches zero, fouling rates follow the same trend as expected since as the velocity approaches zero, the fouling process would tend towards pure diffusion control. For tests using inserts, a velocity maximum in the fouling rate was not clearly observed, as shown in Figure 3.

Much interest has been shown recently in the concept of threshold fouling for crude oils and how this concept can be incorporated into the design of heat exchanger systems [1, 2, 4, 16]. The experimental fouling rate data obtained using either the bare tube or the tube with the insert show similar trends in that as the velocity is increased (beyond that for the maximum fouling rate for bare tubes) the initial fouling rates decrease towards zero. The threshold conditions can therefore be obtained by extrapolating the fouling curves to the axis (Table 2).

3.2 CFD simulation results

3.2.1 CFD simulation for fluid flow in a bare tube

The CFD simulation for the bare tube is straightforward and Figure 4 shows the resulting velocity field. In addition to velocity fields, the Comsol simulation provides solutions to the turbulent viscosity and velocity gradients from which the shear stress distribution can be obtained. Table 3 shows that the values of shear stress obtained from the CFD simulation compare closely with those calculated using the friction factor method [17]. The results are for a tube of 19mm ID and a fluid of viscosity 0.0015 Pas at 150°C. The CFD data are taken at a z position of 0.4m where the turbulence is expected to be fully developed.

3.2.2 CFD simulation for fluid flow in a tube with inserts

The CFD simulations for the tube fitted with a hiTRAN® insert are much more complicated. The insert loop significantly increases the number of mesh elements and therefore the number of loops to be considered must be kept as few as possible. Given its periodical pattern, the number of loops is taken in such a way that the periodical pattern repeats just once. The fluid flow pattern, including the shear stress, would be expected to repeat periodically along the axial direction. Figure 5 shows the resulting velocity field.

With inserts, the shear stress distribution varies significantly in all three dimensions, r, ϕ, and z. Figure 6 shows the shear stress distribution on the wall in the z direction from the edge of a loop located at $z = 0$ as shown in Figure 5 where the loop touches the wall to that over the next loop. The wall shear stress in between the two adjacent loops in the ϕ dimension is quite even compared with that in the z direction shown in Figure 6. Over all dimensions, the wall shear stress drops to the minimum at the wall area just behind the loop edge, as shown in Figure 6. As shown in Table 4, the values of the pressure drop obtained by integrating the CFD simulated data compare well with the experimentally measured values obtained by Cal Gavin. Differences are most likely to be due (i) to slight variations in the way the wires actually position themselves in the tube when compared with the theoretical interpretation in the simulation, and (ii) to how the pressure drop in the CFD simulation is integrated along the axial direction. It is inappropriate to use tube inserts at high bulk velocity since not only would the pressure drop be high but as seen in Figure 2, the fouling rate would in any case be low.

To simplify the simulation, the temperature dependence of the viscosity was not incorporated. This may not significantly undermine the accuracy of the simulation, given the argument as follows: Firstly, the geometry region of relevance in the simulation is very limited. As seen in Figure 5 the horizontal length is just 0.026m. Within this short distance, the temperature variation can be assumed to be negligible. Secondly, for the turbulent flow the total viscosity

is mainly determined by the turbulent viscosity, which is less sensitive to the temperature. However, the temperature effect on the molecular viscosity will be included in further work for CFD simulation of heat transfer in the tube with inserts.

3.3 Modelling fouling rates and threshold conditions

3.3.1 Suppression term as a function of velocity

Attempts to fit a number of models of this type to the experimental data shown in the last section have been made. As an example, the use of Yeap's model [4] with the suppression term, $Cu^{0.8}$ is now described. Yeap's model has been tested since it has been claimed to take into account the effects of both mass transport and chemical reaction in fouling. Indeed, its form follows the fouling-velocity relationship shown in Figure 2:

$$\frac{dR_f}{dt} = \frac{AC_f\, u T_s^{\,2/3} \rho^{2/3} \mu^{-4/3}}{1 + Bu^3 C_f^{\,2} \rho^{-1/3} \mu^{-1/3} T_s^{\,2/3} \exp(E/RT_s)} - Cu^{0.8}$$

The first term of the right hand side of the model represents the fouling resistance increase due to the generation of the fouling deposit, and accounts for the effect of the temperature on the reaction rate as well as the effect of velocity on the mass transfer. Applying this model to all the experimental data (bare tube and tube with insert) yields a poor overall fit as shown in Figure 7. The model parameters obtained by regression are 51.3 (kJ/mol), 8.98×10^{-10} (kg $^{2/3}$K$^{1/3}$ m$^{5/3}$(kW)$^{-1}$s$^{-1/3}$ h^{-1}), 3.81×10^{-5} (m$^{13/3}$kg $^{2/3}$ s$^{8/3}$ K$^{-2/3}$), 1.09×10^{-4} (m$^{6/5}$K s$^{4/5}$ K$^{-2/3}$ (kW)$^{-1}$ h^{-1}) for the model parameters *E*, *A*, *B*, and *C*, respectively. The poor fitting is not surprising since firstly no account is taken of the effect of the insert on the fluid flow pattern, and secondly the model does not account for the effect of the wall shear stress on local fouling rates.

To obtain the threshold conditions from the model, the threshold temperatures for the velocities listed in Table 2 are obtained from the equation when the fouling rate is set to zero. Figure 8 shows that the fitting of threshold conditions is particularly poor. Indeed, it is not possible to draw a unique boundary between the fouling and non-fouling fields. The reason for this is that with mixed fouling data from both bare tube and tube with insert experiments, the fouling threshold temperature is no longer a unique function of the threshold velocity. The threshold temperature may also depend on the tube situation, that is, whether it is bare or whether it is fitted with an insert.

3.3.2 Suppression term as a function of shear stress and equivalent velocity

The best fittings were obtained using Yeap's model, but with the suppression term amended to include shear stress rather than average fluid velocity:

$$\frac{dR_f}{dt} = \frac{A_m C_f\, u T_s^{\,2/3} \rho^{2/3} \mu^{-4/3}}{1 + B_m u^3 C_f^{\,2} \rho^{-1/3} \mu^{-1/3} T_s^{\,2/3} \exp(E/RT_s)} - C_m \tau_w$$

Given that fouling most likely starts in the region of minimum shear stress, it is this stress which should determine the fouling behaviour. Accordingly, the minimum value of shear stress for a given velocity is used in the modified model when fitting the data. As the velocity and velocity related parameters, *Re* and C_f, are strictly defined for round tubes in Yeap's model, the average linear velocity cannot be used directly for a tube with inserts. Hence, the concept of equivalent velocity is introduced. It is defined to be the velocity in a bare tube that gives the same wall shear stress in a tube of the same internal diameter fitted with inserts and operating at a different average fluid velocity. The shear stress and velocity data are obtained

from the CFD simulation. Figure 9 shows the equivalent velocity plot for the 19 mm id tube fitted with a medium density insert. The *Re* and C_f values are then calculated based on the equivalent velocity. The parameter values that give the best fittings are 52.1 (kJ/mol), 7.93×10^{-10} ($kg^{2/3}K^{1/3}\,m^{5/3}(kW)^{-1}s^{-1/3}\,h^{-1}$), 1.80×10^{-5} ($m^{13/3}kg^{2/3}\,s^{8/3}\,K^{-2/3}$), 1.60×10^{-5} ($m^{6/5}K\,s^{4/5}\,K^{-2/3}\,(kW)^{-1}\,h^{-1}$) for E, A_m, B_m, and C_m, respectively. These parameter values are within the ranges reported by Yeap et al. [4]. The parameter E, which is commonly regarded as the activation energy, lies within the range reported previously [6].

Figure 10 shows the fitting of the modified model to the experimental data. The quality of the model fittings is significantly better than that using the linear velocity version of the original Yeap model (Figure 7). As shown in Figure 11, the modified model fits the bare tube experimental data very well. For the case of tube fitted with the insert, the model fits the experimental fouling data reasonably well, as shown in Figure 12.
The model predicted threshold temperatures are obtained as the solution of the modified fouling model equation when the fouling rate is set to zero. The actual velocities are shown in Table 2 and the equivalent velocity for the tube fitted with the insert is obtained using the correlation shown in Figure 9. Figure 13 shows the excellent comparison between the modified model predictions and the experimental threshold conditions. This figure clearly shows that there is now a unique boundary that divides the field into fouling and non-fouling regions, something that the original Yeap model is unable to do. This threshold plot is invaluable in the design of heat exchangers which are subject to fouling.

The concept of equivalent velocity has been shown to be invaluable in extending the Yeap bare tube model to cope with the situation when a hiTRAN® insert is fitted inside a round tube. Hence, it ought to be possible to extend the scope of application of any good bare round tube fouling model to more complex geometries, not only to tubes fitted with inserts but also to non-round flow channels, etc. Moreover, the concept makes it possible to use fouling data generated using simple test rigs for a preliminary prediction of the fouling threshold conditions in a heat exchanger which comprises more complex geometries. Success depends on a viable approach to determine the wall shear stress distribution and CFD is an invaluable tool in this respect.

4 Conclusions and further work

Fouling models that have been developed for simple round tubes cannot be applied directly to more complex geometries, including heat transfer inserts, non-round channels, etc, because the wall shear stress plays a crucial role not only in the fouling process itself but also in the determination of the threshold conditions below which fouling does not take place. Given the practical difficulty in measuring experimentally the wall shear stress in the case of complex geometries, CFD provides a relatively simple alternative provided that the simulated results can be validated using experimental data. In this paper, the concept of equivalent velocity is developed such that a fouling model developed for bare round tubes can be extended for use with more complex geometries. It has been demonstrated, for example, that Yeap's model [4] can be adapted successfully to correlate the data of Maya crude oil fouling in both a bare round tube and a tube fitted with a hiTRAN® insert [6, 9]. Moreover, the fouling threshold conditions for both cases can be predicted successfully, auguring well for the development of successful strategies to mitigate the highly energy consuming fouling problem [4, 9].

Further investigations of fouling in tubes with inserts will mainly focus on simultaneously solving the heat transfer and momentum transfer aspects, as well as addressing the effect of turbulent intensity on the simulation results, and the effect of the inserts on the pressure drop in order to determine the practical scope for insert application. No information is currently available to determine whether fouling could take place on the surface of inserts. However this could form part of further work.

Acknowledgements

The authors are grateful to the UK's Engineering and Physical Sciences Research Council for the award under its Energy Programme of a grant (EP/G059497/1) to study intensified heat transfer for energy saving in the process industries in collaboration with the Centre for Process Integration at the University of Manchester. The authors are also grateful to Cal Gavin Ltd for their support, advice and provision of pressure drop data for their hiTRAN® inserts.

Nomenclature

A, A_m	model parameter
B, B_m	model parameter
C, C_m	model parameter
C_f	Fanning fraction factor
E	activation energy, kJ/mol
R	universal gas constant, 8.314 J/mol K
r	radial coordinate
Re	Reynolds number
R_f	fouling resistance, m^2 K/kW
T_s	surface temperature, K
t	time, s
u	average flow velocity, m/s
z	axial position, m
k	turbulent kinetic energy, m^2/s^2
ε	dissipation rate of turbulent energy, m^2/s^3
μ	fluid dynamic viscosity, Pa.s
ρ	fluid density, kg/m^3
τ_w	wall shear stress, Pa
φ	cylindrical coordinate

References

[1] D.I. Wilson, G.T Polley and S. J. Pugh, Ten years of Ebert, Panchal and the "threshold fouling" concept, Proc. 6th International Conference on Heat Exchanger Fouling and Cleaning: Challenges and Opportunities, Editors Hans Müller-Steinhagen, M. Reza Malayeri and A. Paul Watkinson, Engineering Conferences International, Kloster Irsee, Germany, 2005, pp. 25-36.

[2] W. Ebert and C. B. Panchal, Analysis of Exxon crude-oil, slip-stream coking data, Engineering Foundation Conference on Fouling Mitigation of Heat Exchangers, California, 18–23 June 1995.

[3] N. Epstein, A model of the initial chemical reaction fouling rate for flow within a heated tube and its verification, Proc 10th International Heat Transfer Conference, Institution of Chemical Engineers, Rugby, 1994, Vol. 4, pp. 225-229.

[4] B. L. Yeap, D. I. Wilson, G. T. Polley and S. J. Pugh, Mitigation of crude oil refinery heat exchanger fouling through retrofits based on thermo-hydraulic fouling models. TransIChemE Part A, 82 (2004), pp. 53-71.

[5] B. D. Crittenden, S. A. Hout and N. J. Alderman, Model experiments of chemical reaction fouling, Trans. IChemE Part A, 65 (1987), pp. 165-170.

[6] B. D. Crittenden, S. T. Kolaczkowski, T. Takemoto and D. Z. Phillips, Crude oil fouling in a pilot-scale parallel tube apparatus, *Heat Transfer Engineering*, 30 (2009), pp. 777-785.

[7] B. D. Crittenden., S. T. Kolaczkowski and T. Takemoto, Use of in-tube inserts to reduce fouling from crude oils, AIChE Symp Series, Vol. 89 (No. 295) (1993) pp. 300-307.

[8] J. M. Ritchie and P. Droegemueller, Application of tube inserts in heat exchangers: Benefits of tube inserts, in *Heat exchanger design handbook*, ed. G. F. Hewitt, Begell House, Redding, CT, Section 3.21.2. (2008).

[9] A. W. Krueger and F. Pouponnot, Heat exchanger performance enhancement through the use of tube inserts in refineries and chemical plants – successful application examples: Spirelf, Turbotal and Fixotal systems. Proc. Eurotherm Conference on Fouling and Cleaning in Heat Exchangers, Schladming, Austria, 2009, pp. 400-406.
[10] T. R. Bott, Potential physical methods for the control of biofouling in water system, Trans. IChemE, Part A, 79 (2001), pp. 484-490.
[11] A. Wills, T. R. Bott, and I. J. Gibbard, The control of biofilms in tubes using wire-wound inserts, Canadian J. Chem. Eng., 78 (2000), pp. 61-64.
[12] J. M. Ritchie, P. Droegemueller, and M. J. H. Simmons, hiTRAN® wire matrix inserts in fouling applications, Heat Transfer Engineering. 30 (2009), pp. 876-884
[13] D. Z. Phillips, Mitigation of crude oil fouling by the use of HiTRAN inserts, PhD Thesis, University of Bath (1999).
[14] Comsol Model library - chemical engineering module, 2006, pp. 230-231.
[15] M. Yang, A. Young and B. D. Crittenden, Modelling of the induction period of crude oil fouling, Proc. Eurotherm Conference on Fouling and Cleaning in Heat Exchangers, Schladming, Austria, 2009, pp. 272-280.
[16] Young A, Venditti S, Berrueco C, Yang M, Waters A, Davies H, Hill S, Millan M and Crittenden BD, Characterisation of crude oils and their fouling deposits using a batch stirred cell system, Heat Transfer Engineering, 32 (2011), pp. 216-227.
[17] F. A. Holland and R. Bragg, Fluid flow for Chemical Engineers, Edward Arnold, London, 1995, pp. 70-74.

Table 1 Experimental Conditions

Velocity	Re	Initial (clean) surface temperature			
(m/s)		250°C	265°C	270°C	280°C
0.5	3600	Bare & MDI	Bare & MDI	NA	Bare
0.8	5800	Bare	NA	NA	Bare
1.0	7300	Bare & MDI	Bare & MDI	Bare	Bare
1.5	11000	Bare & MDI	Bare & MDI	Bare	Bare
2.0	14500	Bare & MDI	Bare	Bare	Bare
3.0	21800	Bare	Bare	Bare	Bare
3.6	26200	Bare	Bare	Bare	Bare
4.0	29000	Bare	Bare	Bare	Bare

Bulk temperature: 150°C; Reynolds number calculated for bare tube

Table 2 Fouling Threshold Conditions

Temperature (K)	Linear velocity – bare tube (m/s)	Linear velocity –tube with insert (m/s)
523	4.01	2.23
538	4.16	2.43
543	4.48	No data
553	4.58	No data

Table 3: Comparison of Bare Tube Shear Stresses using CFD and Friction Factor Methods

Velocity (m/s)	Shear stress CFD results (Pa)	Friction factor calculation (Pa)	Re	Friction factor
0.5	0.78	0.82	6909	0.0087
1	2.89	2.77	13818	0.0073
2	9.88	9.31	27636	0.0061
3	19.2	18.93	41455	0.0055
4	32.2	31.33	55273	0.0052

Table 4. Pressure Drops Obtained by CFD Simulation and Measured by Cal Gavin

Linear velocity (m/s)	Pressure drop (kPa/m) hiTRAN®	Pressure drop (kPa/m) CFD simulation
0.5	2.53	4.43
0.8	5.94	6.88
1.0	9.00	13.12
1.6	21.91	25.33
2.0	33.76	38.46

List of Figure Captions

Figure 1: Schematic of the pilot-scale parallel tube apparatus [6]

Three thermocouples are placed in grooves on the tubing outer surface of each test section at 120° separation at each of two axial locations, namely 70mm and 90mm from the tube outlet; these are marked as TI (10-12) and TI (3 - 5), respectively.

Figure 2: Initial fouling rates with the bare tube (bulk temperature: 423K)

Figure 3: Initial fouling rates with medium density insert (bulk temperature: 423K)

Figure 4: Velocity field obtained from CFD simulation for bare tube (linear velocity: 4m/s)

Figure 5: CFD simulation results for the velocity field (linear velocity: 1.0 m/s)

Left end: inlet; Right end: outlet

Figure 6: Wall shear stress distribution from the edge of one loop to that of the next

Figure 7: Comparison of experimental fouling rate data to the Yeap model predictions

Figure 8: Experimental threshold conditions compared with Yeap model predictions

Figure 9: Equivalent velocity of the 19 mm id tube flow with the medium density insert

Figure 10: Experimental threshold conditions compared with modified Yeap model predictions

Figure 11 Comparison of bare tube experimental data and the modified model predictions at a constant wall temperature (523K)

Symbols: Experimental data; Line: Model fit

Figure 12: Comparison of the insert experimental data and the modified model predictions at a constant wall temperature (523K) for the tube fitted with the medium density insert

Figure 13: Threshold conditions – temperature versus velocity/equivalent velocity

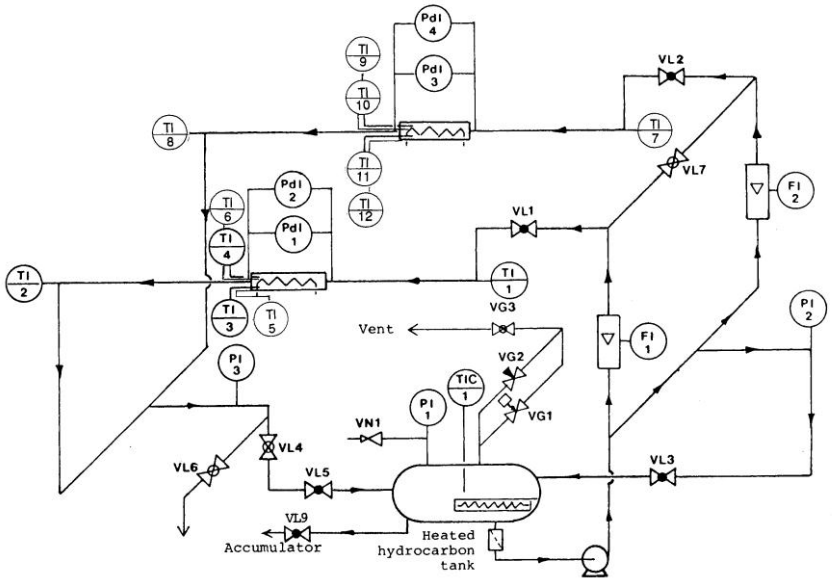
PdI 4
TI 9
PdI 3
TI 10
VL2
TI 8
TI 7
TI 11
VL7
FI 2
PdI 2
TI 6
TI 12
VL1
PdI 1
TI 4
TI 2
TI 1
VG3
TI 3
TI 5
Vent
FI 1
PI 2
PI 3
VG2
TIC 1
PI 1
VG1
VN1
VL4
VL3
VL6
VL5
VL9
Accumulator
Heated
hydrocarbon
tank

Figure. 1

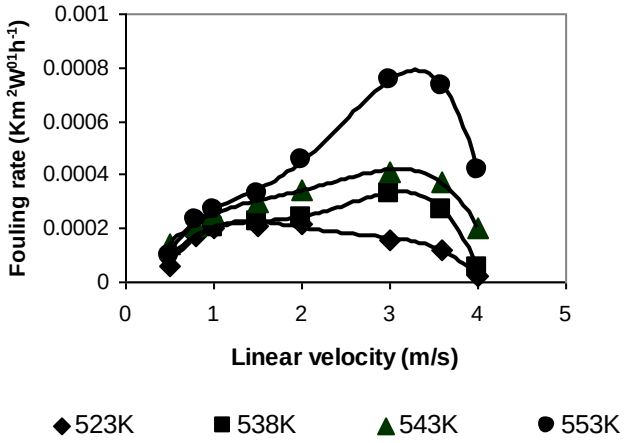
0.001
0.0008
0.0006
0.0004
0.0002
0
Fouling rate (Km²W⁰¹h⁻¹)
0
1
2
3
4
5
Linear velocity (m/s)
523K
538K
543K
553K

Figure 2

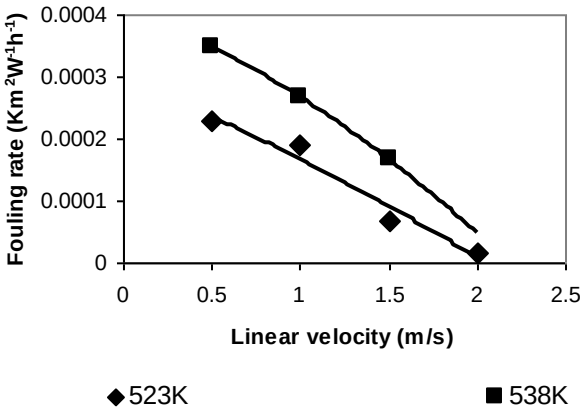
0.0004
0.0003
0.0002
0.0001
0
Fouling rate (Km²W⁻¹h⁻¹)
0
0.5
1
1.5
2
2.5
Linear velocity (m/s)
523K
538K

Figure 3

Axially symmetric geometry, the upper boundary representing the central axis.
Left end: inlet; Right end: outlet

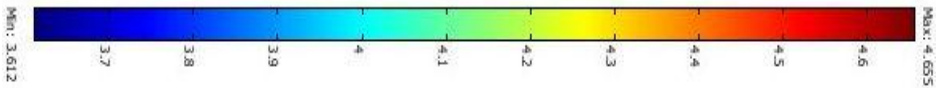

Velocity scale (m/s)

Figure 4

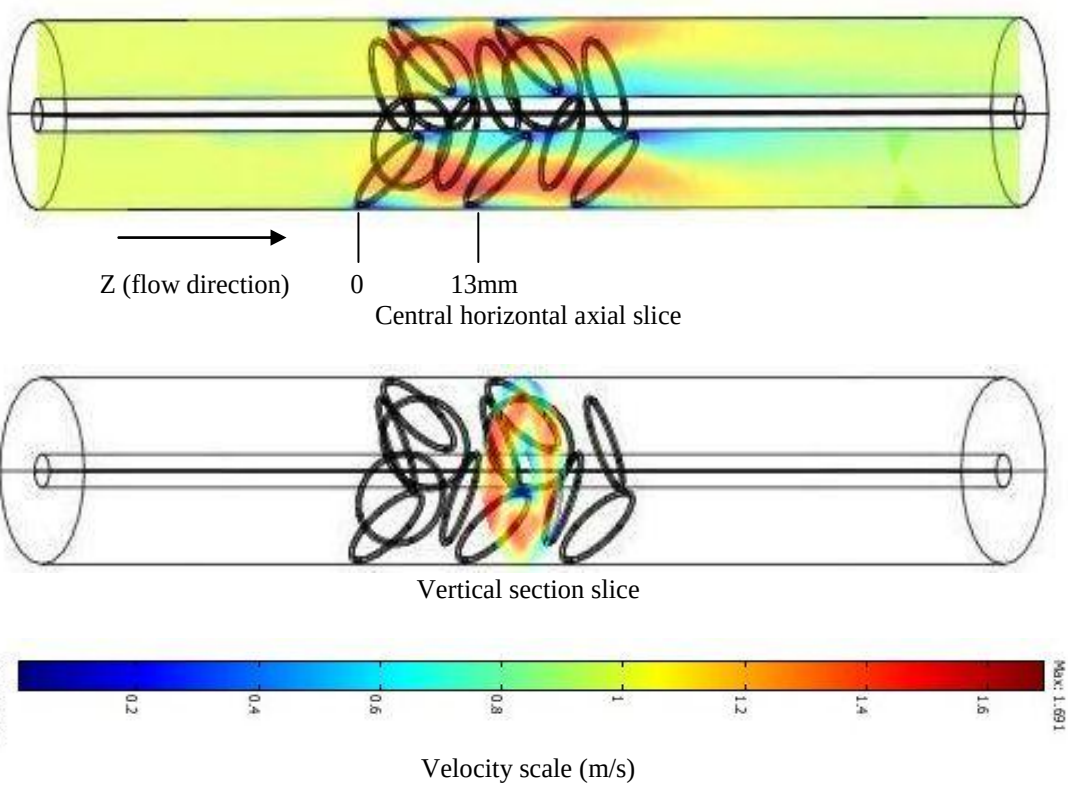
Z (flow direction)
0
13mm
Central horizontal axial slice
Vertical section slice
Min: 6.887e-3
0.2
0.4
0.6
0.8
1
1.2
1.4
1.6
Max: 1.691
Velocity scale (m/s)

Figure 5

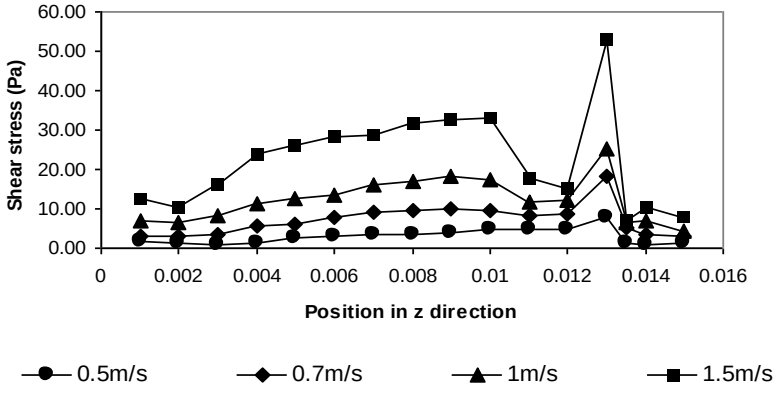
60.00
50.00
40.00
30.00
20.00
10.00
0.00
Shear stress (Pa)
0
0.002
0.004
0.006
0.008
0.01
0.012
0.014
0.016
Position in z direction
0.5m/s
0.7m/s
1m/s
1.5m/s

Figure 6

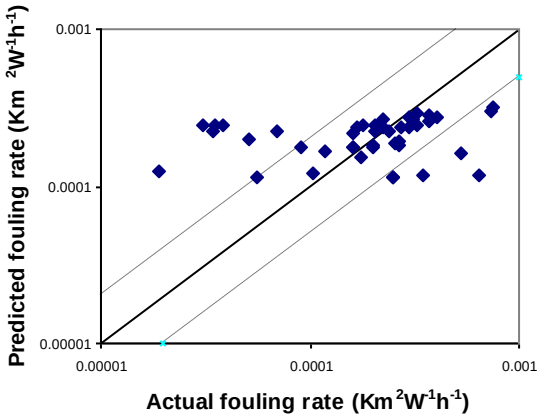
Predicted fouling rate (Km ²W⁻¹h⁻¹)
0.001
0.0001
0.00001
0.00001
0.0001
0.001
Actual fouling rate (Km²W⁻¹h⁻¹)

Figure 7

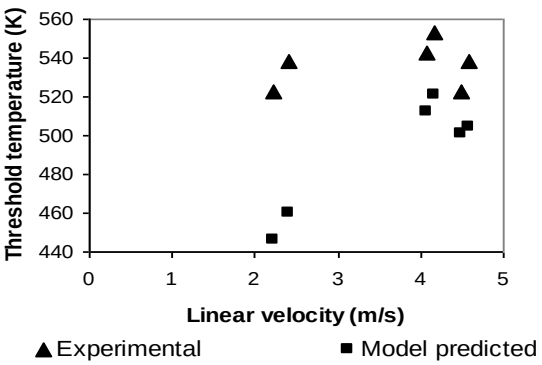
Threshold temperature (K)
560
540
520
500
480
460
440
0
1
2
3
4
5
Linear velocity (m/s)
Experimental
Model predicted

Figure 8

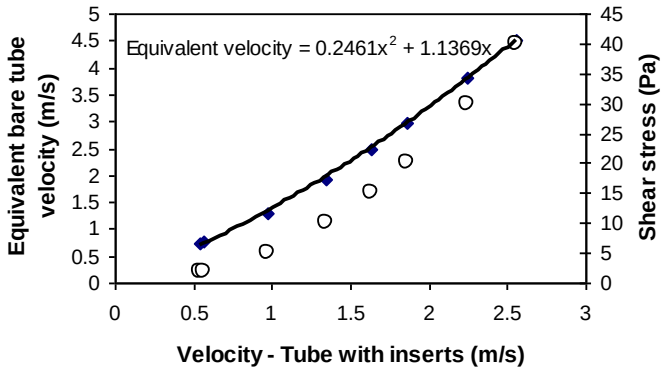

■: Velocity; ¤: Shear stress

Figure 9

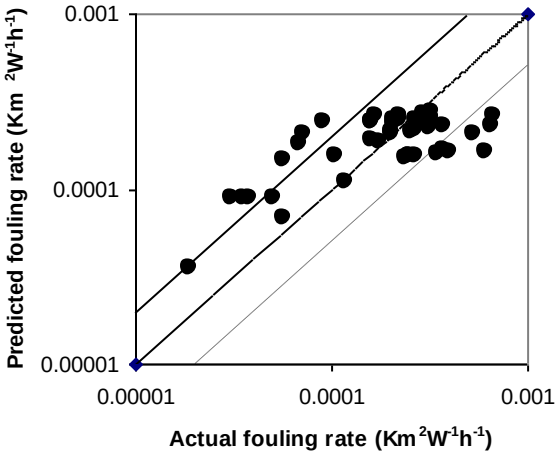
0.001
0.0001
0.00001
Predicted fouling rate (Km ²W⁻¹h⁻¹)
0.00001
0.0001
0.001
Actual fouling rate (Km²W⁻¹h⁻¹)

Figure 10

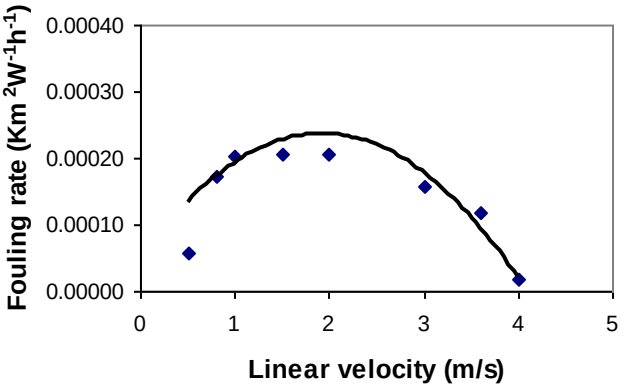
Fouling rate (Km 2W-1h-1)
0.00040
0.00030
0.00020
0.00010
0.00000
0
1
2
3
4
5
Linear velocity (m/s)

Figure 11

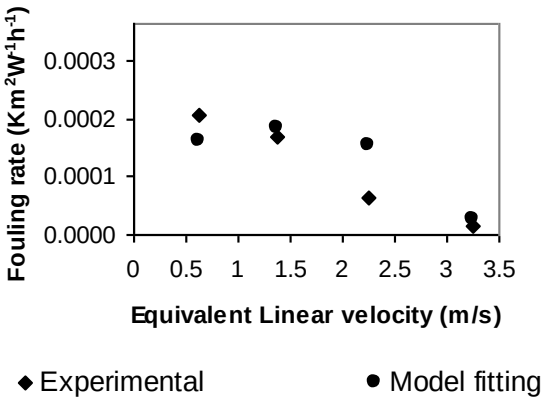
Fouling rate (Km2W-1h-1)
0.0003
0.0002
0.0001
0.0000
0
0.5
1
1.5
2
2.5
3
3.5
Equivalent Linear velocity (m/s)
Experimental
Model fitting

Figure 12

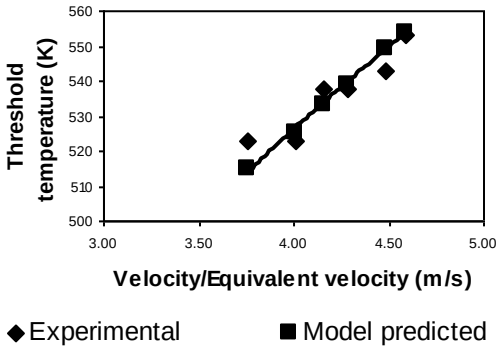
Threshold temperature (K)
560
550
540
530
520
510
500
3.00
3.50
4.00
4.50
5.00
Velocity/Equivalent velocity (m/s)
Experimental
Model predicted

Figure 13